Other Nanotechnology Publications   Birck Nanotechnology Center

5-1-2008

Band-Structure Effects on the Performance of III-V Ultrathin-Body SOI MOSFETs

Yang Liu
Purdue University - Main Campus

Neophytos Neophytou
Purdue University - Main Campus

Gerhard Klimeck
Purdue University - Main Campus, gekco@purdue.edu

Mark S. Lundstrom
Purdue University - Main Campus

Follow this and additional works at: http://docs.lib.purdue.edu/nanodocs

Band-Structure Effects on the Performance of III–V Ultrathin-Body SOI MOSFETs

Yang Liu, *Student Member, IEEE*, Neophytos Neophytou, *Student Member, IEEE*,
Gerhard Klimeck, *Senior Member, IEEE*, and Mark S. Lundstrom, *Fellow, IEEE*

Abstract—This paper examines the impact of band structure on deeply scaled III–V devices by using a self-consistent 20-band sp^{3}d^{5}s*-SO semiempirical atomistic tight-binding model. The density of states and the ballistic transport for both GaAs and InAs ultrathin-body n-MOSFETs are calculated and compared with the commonly used bulk effective mass approximation, including all the valleys (Γ, X, and L). Our results show that for III–V semiconductors under strong quantum confinement, the conduction band nonparabolicity affects the confinement effective masses and, therefore, changes the relative importance of different valleys. A parabolic effective mass model with bulk effective masses fails to capture these effects and leads to significant errors, and therefore, a rigorous treatment of the full band structure is required.

Index Terms—Band structure, effective mass, injection velocity, MOSFETs, nonparabolicity, quantum confinement, tight binding (TB), ultrathin body (UTB), III–V.

I. INTRODUCTION

OVER THE past decades, CMOS technology has been largely geared toward improving MOSFET performance and increasing device density through aggressive scaling of their feature sizes. For present-day very large scale integration technology at the 65-nm node and beyond, power consumption has become the bottleneck for further scaling. To circumvent this limitation, new device structures and materials are being pursued. New channel materials, such as Ge and III–V semiconductors, are being investigated as high-mobility channel materials for high-performance CMOS with novel process techniques such as atomic layer deposition, high-κ dielectrics, and metal gates [1].

The theoretical study of quasi-ballistic devices with new channel materials is a challenge because quantum effects become important in thin inversion layers, and they must be treated together with band structure and electrostatics. The effective mass approximation (EMA) has been widely used to study transport in these nanoscale devices with Si, Ge, and alternative channel materials and various surface/transport orientations, both in the ballistic limit [2]–[7] and in the presence of carrier scattering [8]. Recent work has shown that using the bulk effective masses is reasonably accurate for silicon
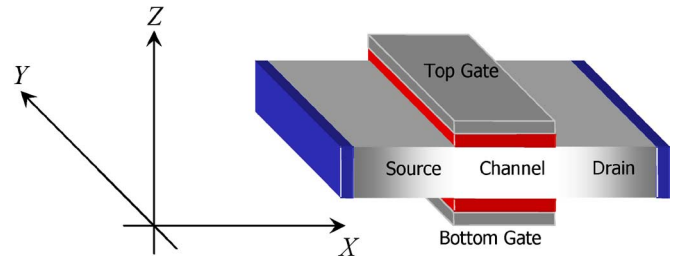
Fig. 1. DG-UTB device structure simulated in this paper. The transport, width, and wafer orientations are along the X-, Y-, and Z-axes, respectively.

n-MOSFETs with an ultrathin body (UTB) [9], [10]. It is still not clear, however, whether bulk effective masses can still be used for III–V UTB structures. It has long been known for high-bias quantum-effect-dominated devices, such as high-performance resonant tunneling diodes in III–V materials, that effective mass calculations cannot lead the accurate performance analysis and prediction [11]. A tight-binding (TB) model that captures band nonparabolicities, band-to-band coupling, and states throughout the Brillouin zone was needed to predict and explain current flow through room temperature, high current density, and high-bias RTDs [11]. By adopting a 20-band sp^{3}d^{5}s*-SO semiempirical atomistic TB model with a self-consistent Poisson solver, we explore in this paper the band-structure effects on the ballistic performance of GaAs and InAs n-MOSFETs with a UTB structure and compare the results with the bulk EMA. Our results show that the nonparabolicity, which shifts the subband-energy levels and changes the in-plane effective masses, becomes important for the III–V UTB structures where quantum confinement is strong and affects the relative importance of different valleys (Γ, X, and L). As a result, the use of bulk effective masses in III–V MOSFETs can lead to large errors.

This paper is organized as follows. Section II illustrates the nonparabolicity in the band structure for GaAs/InAs UTB structures with a TB approach. In Section III, quantities related with ballistic transport, such as drain–current, inversion charge, and injection velocities, are calculated self-consistently with the TB band structure; the results are then compared and discussed with those achieved through the parabolic bulk effective mass approach. Section IV summarizes this paper.

II. NONPARABOLICITY IN III–V UTB BAND STRUCTURES

The simulated device with symmetrical double-gate (DG) and intrinsic UTB is shown in Fig. 1. The transport, transverse,

TABLE I
(a) Transport, Transverse, and Confinement Effective Masses and Subband Degeneracies of (100)/⟨100⟩ III–V n-MOSFETs From the Bulk Principal Effective Masses for Each Valley. (b) Numerical Values of the Transport, Transverse, and Confinement Effective Masses and Subband Degeneracies of (100)/⟨100⟩ n-MOSFETs for GaAs and InAs From the Bulk Principal Effective Masses for Each Valley

Valley	g	m_x	m_y	m_z
Γ	1	m_Γ	m_Γ	m_Γ
X_1	1	m_{Xt}	m_{Xt}	m_{Xl}
X_2	1	m_{Xt}	m_{Xl}	m_{Xt}
	1	m_{Xl}	m_{Xt}	m_{Xt}
L	4	$m_{Lt}\dfrac{2m_{Ll}+m_{Lt}}{2m_{Lt}+m_{Ll}}$	$\dfrac{m_{Ll}+2m_{Lt}}{3}$	$\dfrac{3m_{Ll}m_{Lt}}{2m_{Ll}+m_{Lt}}$

(a)

	GaAs				InAs			
Valley	g	m_x	m_y	m_z	Valley	g	m_x	m_y	m_z
Γ	1	0.0670	0.0670	0.0670	Γ	1	0.0239	0.0239	0.0239
X_1	1	0.2300	0.2300	1.3000	X_1	1	0.2300	0.2300	1.3000
X_2	1	0.2300	1.3000	0.2300	X_2	1	0.2300	1.3000	0.2300
	1	1.3000	0.2300	0.2300		1	1.3000	0.2300	0.2300
L	4	0.1425	0.6836	0.1109	L	4	0.1425	0.6836	0.1109

(b)

and wafer orientations are along the X-, Y-, and Z-axes, respectively. The 2-D band structures for III–V channel materials of GaAs and InAs are calculated by using a semiempirical TB model, where 20 orbitals consisting of an $sp^3d^5s^*$ basis with spin–orbit coupling are used to represent each atom along the body thickness in the UTB Hamiltonian [12]–[15]. The TB coupling parameters have been optimized to accurately reproduce the bandgap and the effective masses of the bulk material [13], [14]. A hard wall boundary condition at the top and bottom interfaces is applied by removing the dangling bonds with a technique similar to hydrogen passivation of $Si-SiO_2$ interfaces [16]. Two different body thicknesses are chosen for GaAs in this paper: $t_{GaAs} = 5.5$ and 2.6 nm, which are the 2016 and 2020 International Technology Roadmap for Semiconductors technology nodes, respectively [17]. For InAs, we study only $t_{InAs} = 2.6$ nm for which the differences between the TB and bulk EMA approaches are large.

The band structure and the density of states (DOS) of III–V UTB with (100) confinement direction are first calculated for a thin film at $V_G = 0$, i.e., a flatband condition. The TB parameters and the bulk effective masses that we use for GaAs and InAs in this paper are from [14]. The bandgaps for GaAs and InAs are 1.424 and 0.37 eV, respectively. For comparison, we also calculate the DOS using the parabolic effective mass model with bulk effective masses taken from the same TB model. The transport, transverse, and confinement effective masses (see [18] and [19]) with the corresponding bulk values for each valley are listed in Table I(a) and (b).

The computed DOS and $E - k$ are shown in Figs. 2 and 3 for the two GaAs thin films of 5.5 and 2.6 nm, respectively. For the thicker body ($t_{GaAs} = 5.5$ nm), both the TB and bulk EMA approaches show that the Γ valley has the smallest DOS effective mass and the lowest energy. For the $t_{GaAs} = 2.6$-nm structure for which quantum confinement is stronger, the bulk EMA shows that X_1 valley is the lowest in energy because the Γ valley subband increases with strong quantum confinement. The TB results, however, predict that the Γ valley is still the

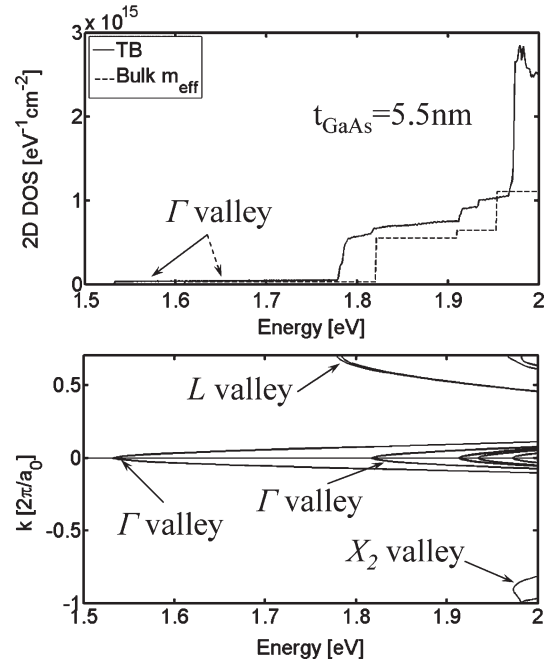

Fig. 2. DOS (TB and bulk EMA) and band structure (TB) calculated for $t_{GaAs} = 5.5$-nm UTB. Both the TB and the bulk EMA show that the Γ valley has the smallest DOS effective mass and the lowest energy. The bulk conduction band edge is at 1.424 eV.

lowest in energy. Similar results are observed in the InAs thin film in Fig. 4, where the differences between the TB and bulk EMA approaches are even larger. For $t_{InAs} = 2.6$ nm, the Γ valley is the lowest in energy according to TB, but the bulk EMA shows the L valley as the lowest in energy.

The discrepancy between the TB and bulk EMA results shown in Figs. 2–4 is due to the nonparabolicity of the Γ valley in GaAs and InAs. The Γ valley confinement effective masses (m_z), as deduced from the TB calculations, are plotted as a function of the thin-film thickness in Fig. 5. For both GaAs and InAs, we observe that m_z increases as the UTB gets thinner.
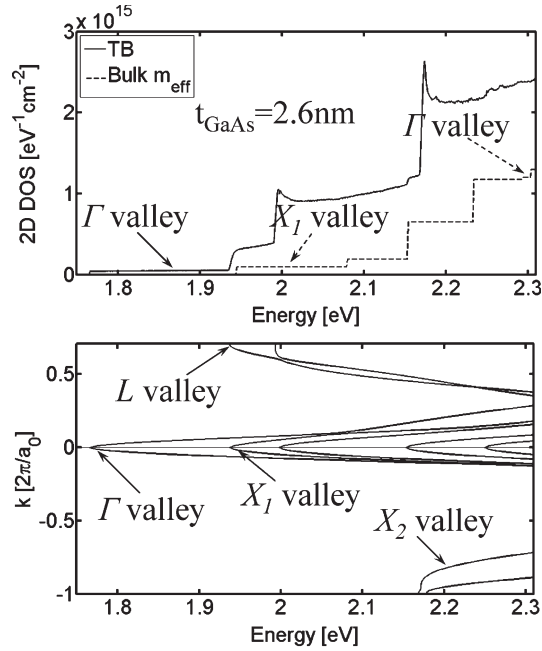
Fig. 3. DOS (TB and bulk EMA) and band structure (TB) calculated for $t_{GaAs} = 2.6$-nm UTB. The TB results show that the Γ valley is still the most important, whereas the bulk EMA show that the X_1 valley becomes the most important with strong quantum confinement.
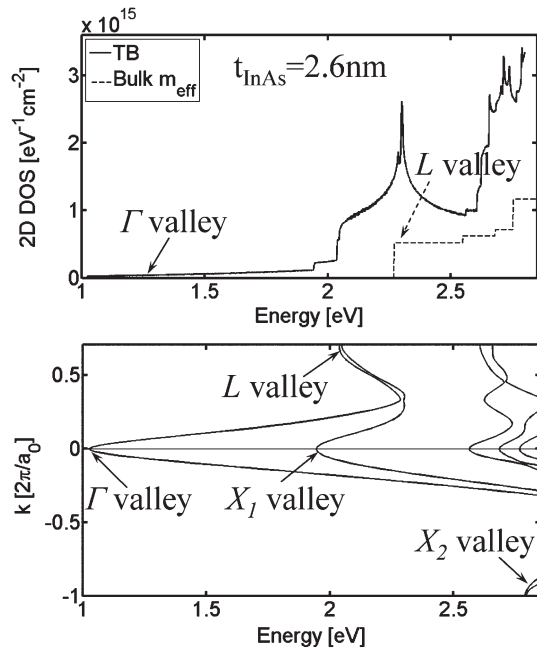

Fig. 4. DOS (TB and bulk EMA) and band structure (TB) calculated for $t_{InAs} = 2.6$ nm UTB. The TB model shows that the Γ valley still dominates the transport, whereas by the bulk EMA model, the L valley is the most important. The bulk conduction band edge is at 0.596 eV.

As a result, the Γ valley subband-energy levels do not increase as much as would be expected from a parabolic effective mass model. The confinement effective mass m_z converges to the bulk values when the film thickness gets to less than 30 nm. The conclusion is that the Γ valley subbands are the most important for even very thin III–V films—in sharp contrast to the predictions of the bulk EMA. These results have a
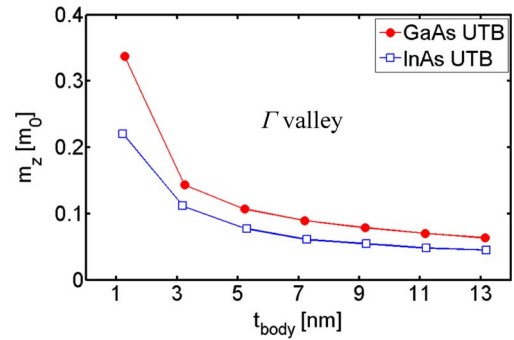

Fig. 5. Confinement effective mass m_z of the Γ valley as a function of the thin-film body thickness for GaAs and InAs. For both semiconductor materials, m_z increases significantly as the body thickness decreases.

substantial effect on the predicted I–V characteristics of III–V MOSFETs.

III. DEVICE PERFORMANCE AND DISCUSSION

The effect of conduction band nonparabolicity on the ballistic I–V characteristics of III–V UTB SOI $(100)/\langle 100 \rangle$ n-MOSFETs is studied in this section. The band structure of GaAs/InAs UTB n-MOSFETs is first calculated self-consistently versus gate voltage by coupling the TB model and the Poisson equation. The ballistic I–V characteristic is then calculated by using a semiclassical FET model at the top of the barrier [20]. Specifically, the group velocity of each state is calculated from the tabulated TB $E - k$ data of the UTB, and the carrier density is then evaluated by assuming that the states with a positive (negative) group velocity are in equilibrium with the source (drain) reservoir. The drain–current is then readily obtained by taking the difference between the source and drain fluxes, and the inversion charge is determined by summing up the carriers injected from the source and the drain. For comparison, we also calculate the ballistic I–V characteristics using a parabolic $E - k$ with bulk effective masses. The symmetric, DG, and intrinsic body III–V UTB n-MOSFET device simulated in this paper has an EOT $= t_{SiO_2} = 0.5$ nm, with $V_{DD} = 0.8$ V for $t_{GaAs} = 5.5$ nm and $V_{DD} = 0.5$ V for $t_{GaAs/InAs} = 2.6$ nm separately. For both body thicknesses, I_{OFF} is adjusted to 0.11 $\mu A/\mu m$ in TB by varying the gate work functions, and the Fermi level in the bulk EMA is fixed the same with the TB for a direct comparison. All simulations are assumed to be at 300 K.

Fig. 6(a)–(d) shows the computed ballistic current, charge density, and injection velocities for $t_{GaAs} = 5.5$ nm. Due to the small effect of nonparabolicity in this relatively thick body, the use of bulk effective masses gives reasonably accurate results as compared with the TB model. A shift in the threshold voltage is observed between the TB and the bulk EMA, which arises from the increase in the confinement effective mass in the Γ valley by TB, as it was observed in Fig. 5. The computed band structure and the DOS at $V_G = 0.65$ V, where $N_{inv} = 0.98 \times 10^{13}/cm^2$ by TB model, are shown in Fig. 7. The location of the Fermi level shows that the Γ valley dominates the device performance, but the heavier L valley is also beginning to be
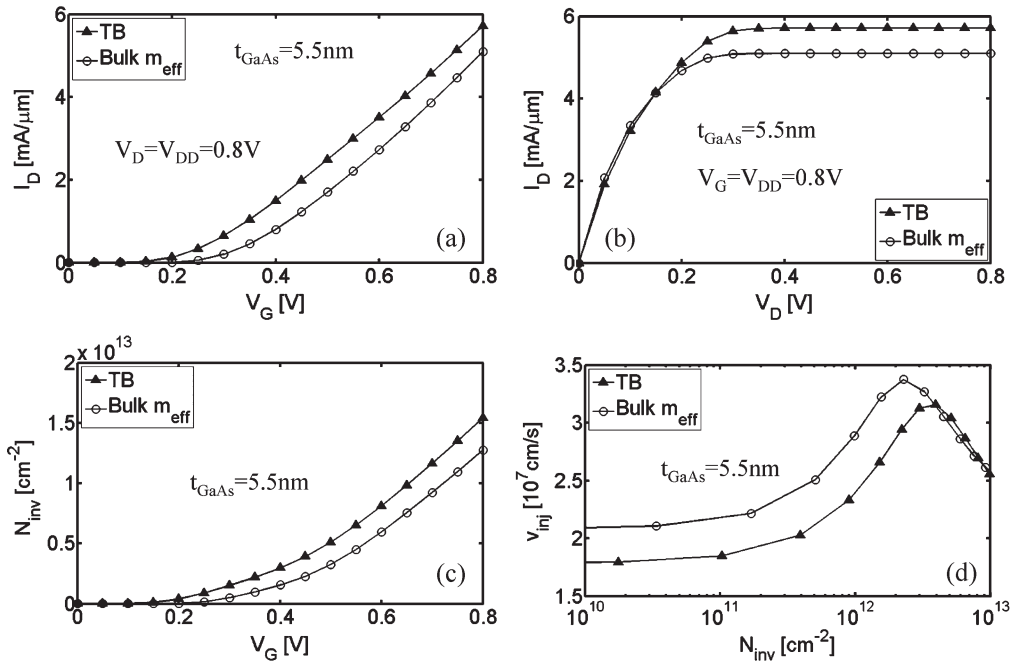
Fig. 6. (a) and (b) Self-consistent results of the $I–V$, (c) charge density, and (d) ballistic injection velocity for $t_{GaAs} = 5.5$ nm, calculated by the TB model and the bulk EMA. The bulk EMA gives reasonably accurate results compared with the TB due to the small nonparabolicity.
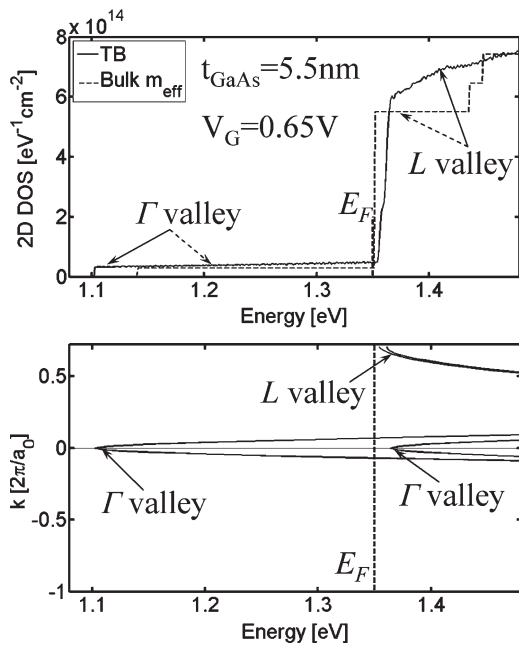

Fig. 7. Band structure and DOS for $t_{GaAs} = 5.5$ nm at $V_G = 0.65$ V. The Γ valley is shown to be the most important in transport. At deep inversion, the L valleys begin to conduct carriers and lead to a decrease in the injection velocity.

populated. For thinner bodies, we expect to see more significant difference between the TB and the EMA approaches.

Fig. 8(a)–(d) shows the computed current, charge density, and injection velocities for the thin-body GaAs structure. Very substantial (more than a factor of two in some cases) differences between the TB and the effective mass models are observed. With a bulk effective mass model, the Γ valley subband energy is higher than the X_1 subbands, which makes the X_1 subbands dominant in transport. The TB model, however, predicts that the Γ valley dominates. The difference between the two models is

most clearly shown in Fig. 8(d), which compares the injection velocities versus the charge density. Fig. 9 shows the valley population versus the charge density for the TB and EMA approaches. Fig. 9(a) shows the importance of X_1 subbands for the effective mass model, whereas Fig. 9(b) shows that in the TB model, the Γ valley dominates until the L valleys begin to conduct under a very strong inversion. This is also shown in Fig. 10, which plots the DOS and the band structure at $V_G = 0.5$ V.

Finally, it is interesting to ask whether an effective mass model with appropriate body-thickness-dependent effective masses could be used. From the energy independence in the DOS in Fig. 7, we observe that the subband formed from the Γ valley is quite parabolic in the $k_x–k_y$ plane (although the confinement effective mass m_z changes due to the nonparabolicity in the bulk band structure), which enables us to extract fairly accurate in-plane effective masses (m_x, m_y) by fitting a parabola from the bottom of the band to the energy at the Fermi level. These extracted effective masses (m_x, m_y, m_z) for the UTB are then used to recalculate the ballistic $I–V$ characteristics, and the results are shown in Fig. 8(a)–(d) in squares. The results match with those by TB quite well, indicating that a thickness-dependent effective mass model can be used for device analysis of GaAs UTB structures. For each structure, however, one first needs to compute the band structure and extract the effective masses.

The InAs UTB n-MOSFET was also explored. As discussed earlier, according to the effective mass model with bulk effective masses, the Γ valley energy increases so much that it becomes irrelevant. The TB model, however, shows that the confinement effective mass increases significantly so that the subbands formed from the Γ valley remain the most important even under high injection. Fig. 11(a)–(d) shows the ballistic $I–V$ results for $t_{InAs} = 2.6$ nm. It is seen that the use of
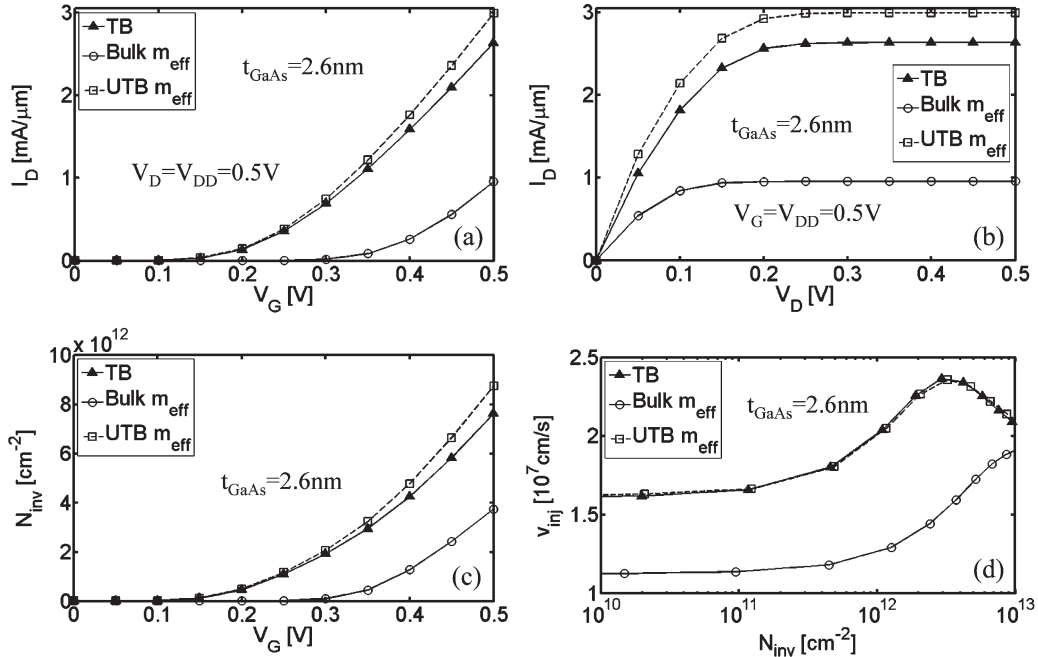
Fig. 8. (a) and (b) Self-consistent results of the $I\text{–}V$, (c) charge density, and (d) ballistic injection velocity for $t_{\mathrm{GaAs}} = 2.6$ nm, calculated by the TB model and the bulk EMA. The bulk EMA results differ from those of the TB significantly due to the large nonparabolicity in the Γ valley in the thin film.
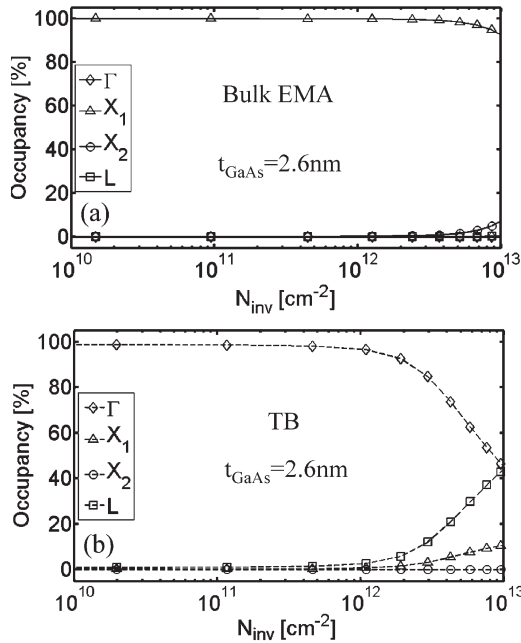

Fig. 9. Different valley occupancies as a function of the channel density by (a) the bulk EMA and (b) the TB model. The Γ valley subbands remain the most important in transport due to the large nonparabolicity effects.
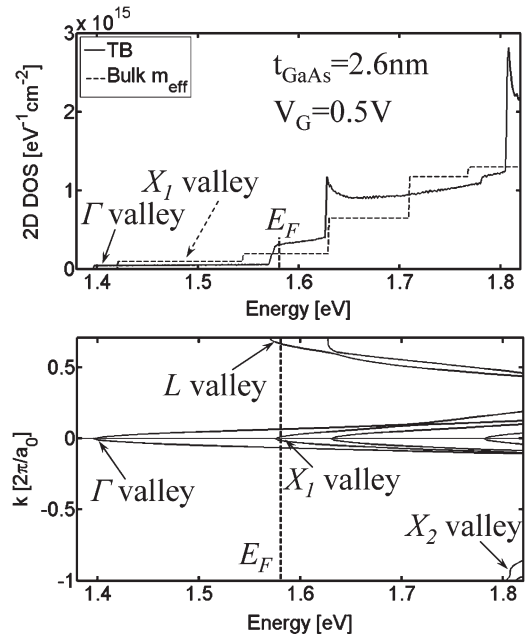

Fig. 10. Band structure and DOS for $t_{\mathrm{GaAs}} = 2.6$ nm at $V_G = 0.5$ V. The Γ valley is shown to be the most important in transport by the TB, but the bulk EMA predicts that the X_1 valleys have more importance.

bulk effective masses leads to large errors as compared with the TB results. The threshold voltage by the EMA is more than 1 V higher than that by the TB, which is shown in Fig. 11(a) and (b). According to the bulk EMA, the device is not even turned on at $V_G = V_{\mathrm{DD}} = 0.5$ V. Furthermore, since the heavy L valley dominates the transport in bulk EMA model, the carrier injection velocity is much smaller than the TB results. We can, however, extract the confinement effective mass (from the TB subband-energy level with no gate bias) and

the in-plane effective masses (by fitting the bottom of the TB band structure with a parabola) of the Γ valley. The results, which are shown as squares in Fig. 11(a)–(d), match with the TB well, except for divergence of the injection velocity under strong inversion. The smaller injection velocity of the TB model is a result of the increased transport mass caused by the in-plane nonparabolicity. This effect is also seen in the DOS plot at $V_G = 0.5$ V, as shown in Fig. 12. Therefore, a parabolic effective mass should not be used for InAs.
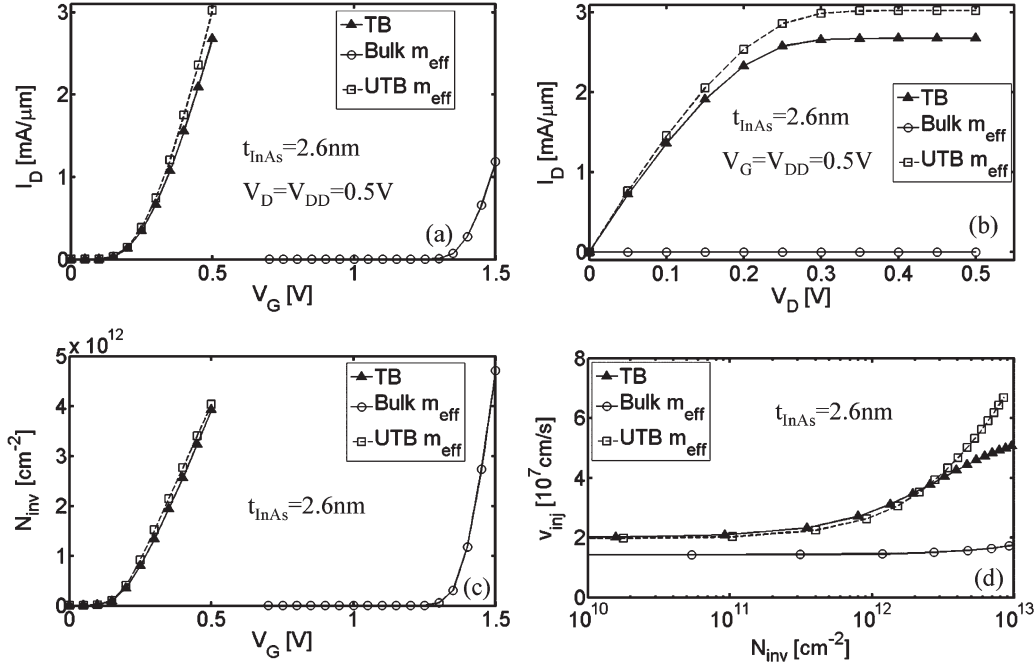
Fig. 11. Self-consistent results of the (a) and (b) I–V, (c) charge density, and (d) ballistic injection velocity for $t_{InAs} = 2.6$ nm, calculated by TB, bulk EMA, and UTB EMA. The bulk EMA results lead to large errors due to the significant nonparabolicity in the very thin body.
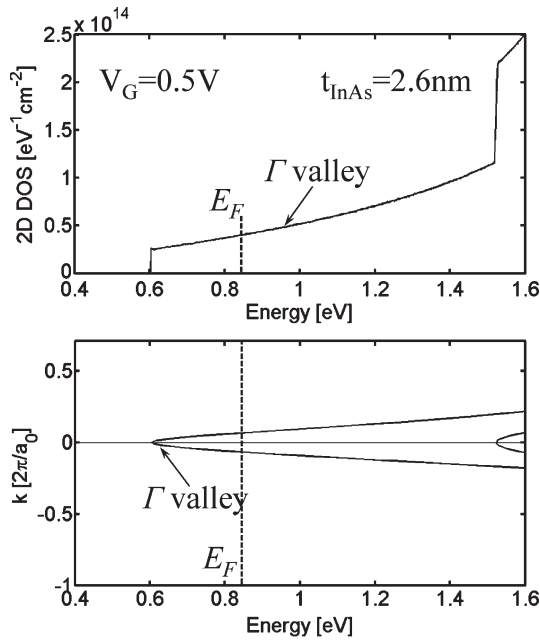
Fig. 12. DOS and band structure for $t_{InAs} = 2.6$ nm at $V_G = 0.5$ V by the TB. Large in-plane nonparabolicity is observed in the Γ valley subbands, with the slope in the 2-D DOS plot.

IV. CONCLUSION

In this paper, we examined the question of how band structure affects the performance of the III–V UTB n-MOSFETs. We used an $sp^3d^5s^*$ TB model and compared the results to a parabolic effective mass model with effective masses taken from the bulk. We found that for UTB structures with III–V channel materials, nonparabolicity in the Γ valley plays an important role and significantly affects the device performance by changing the relative importance of different valleys. The use of

bulk effective masses in a III–V UTB MOSFET overestimates the importance of the X_1 and L valleys, whereas a significant Γ valley population is, in fact, observed in the TB calculations. Bulk effective masses should, therefore, never be used in the analyses of III–V UTB. As an alternative, thickness-dependent effective masses may be used. This works well for GaAs, but in-plane nonparabolicity is important for InAs and is not captured by such a model. The use of a rigorous band structure may be important to quantitatively assess the performance of III–V MOSFETs.

REFERENCES

[1] P. D. Ye, G. D. Wilk, B. Yang, J. Kwo, S. N. G. Chu, S. Nakahara, H. J. L. Gossmann, J. P. Mannaerts, M. Hong, K. K. Ng, and J. Bude, "GaAs metal–oxide–semiconductor field-effect transistor with nanometer-thin dielectric grown by atomic layer deposition," *Appl. Phys. Lett.*, vol. 83, no. 1, pp. 180–182, Jul. 2003.

[2] S. E. Laux, "Simulation study of Ge n-channel 7.5 nm DGFETs of arbitrary crystallographic alignment," in *IEDM Tech. Dig.*, 2004, pp. 135–138.

[3] A. Pethe, T. Krishnamohan, D. Kim, S. Oh, H.-S. P. Wong, Y. Nishi, and K. C. Saraswat, "Investigation of the performance limits of III–V double-gate n-MOSFETs," in *IEDM Tech. Dig.*, 2005, pp. 605–608.

[4] M. De Michielis, D. Esseni, and F. Driussi, "Analytical models for the insight into the use of alternative channel materials in ballistic nano-MOSFETs," *IEEE Trans. Electron Devices*, vol. 54, no. 1, pp. 115–123, Jan. 2007.

[5] T. Low, Y. T. Hou, M. F. Li, C. Zhu, A. Chin, G. Samudra, L. Chan, and D.-L. Kwong, "Investigation of performance limits of germanium double-gated MOSFETs," in *IEDM Tech. Dig.*, 2003, pp. 691–694.

[6] F. Assad, Z. B. Ren, D. Vasileska, S. Datta, and M. Lundstrom, "On the performance limits for Si MOSFETs: A theoretical study," *IEEE Trans. Electron Devices*, vol. 47, no. 1, pp. 232–240, Jan. 2000.

[7] K. Natori, "Ballistic metal–oxide–semiconductor field effect transistor," *J. Appl. Phys.*, vol. 76, no. 8, pp. 4879–4890, Oct. 1994.

[8] R. Venugopal, S. Goasguen, S. Datta, and M. S. Lundstrom, "Quantum mechanical analysis of channel access geometry and series resistance in nanoscale transistors," *J. Appl. Phys.*, vol. 95, no. 1, pp. 292–305, Jan. 2004.

[9] J. L. van der Steen, D. Esseni, P. Palestri, L. Selmi, and R. J. E. Hueting, "Validity of the parabolic effective mass approximation in silicon and germanium n-MOSFETs with different crystal orientations," *IEEE Trans. Electron Devices*, vol. 54, no. 8, pp. 1843–1851, Aug. 2007.

[10] Y. Liu, N. Neophytou, T. Low, G. Klimeck, and M. S. Lundstrom, "A tight-binding study of the ballistic injection velocity for ultrathin-body SOI MOSFETs," *IEEE Trans. Electron Devices*, vol. 55, no. 3, pp. 866–871, Mar. 2008.

[11] G. Klimeck, R. Lake, D. Blanks, C. L. Fernando, C. Bowen, T. Moise, and Y. C. Kao, "The effects of electron screening length and emitter quasi-bound states on the polar-optical phonon scattering in resonant tunneling diodes," *Phys. Status Sol. B, Basic Res.*, vol. 204, no. 1, pp. 408–411, Nov. 1997.

[12] J. M. Jancu, R. Scholz, F. Beltram, and F. Bassani, "Empirical spds* tight-binding calculation for cubic semiconductors: General method and material parameters," *Phys. Rev. B, Condens. Matter*, vol. 57, no. 11, pp. 6493–6507, Mar. 1998.

[13] G. Klimeck, R. C. Bowen, T. B. Boykin, C. Salazar-Lazaro, T. A. Cwik, and A. Stoica, "Si tight-binding parameters from genetic algorithm fitting," *Superlattices Microstruct.*, vol. 27, no. 2, pp. 77–88, Feb. 2000.

[14] T. B. Boykin, G. Klimeck, R. C. Bowen, and F. Oyafuso, "Diagonal parameter shifts due to nearest-neighbor displacements in empirical tight-binding theory," *Phys. Rev. B, Condens. Matter*, vol. 66, no. 12, pp. 125 207–125 212, Sep. 2002.

[15] G. Klimeck, S. S. Ahmed, H. Bae, N. Kharche, R. Rahman, S. Clark, B. Haley, S. H. Lee, M. Naumov, H. Ryu, F. Saied, M. Prada, M. Korkusinski, and T. B. Boykin, "Atomistic simulation of realistically sized nanodevices using NEMO 3-D—Part I: Models and benchmarks," *IEEE Trans. Electron Devices*, vol. 54, no. 9, pp. 2079–2089, Sep. 2007.

[16] S. Lee, F. Oyafuso, P. von Allmen, and G. Klimeck, "Boundary conditions for the electronic structure of finite-extent embedded semiconductor nanostructures," *Phys. Rev. B, Condens. Matter*, vol. 69, no. 4, pp. 045 316–045 323, Jan. 2004.

[17] *International Technology Roadmap for Semiconductors* [Online]. Available: http://public.itrs.net

[18] A. Rahman, M. S. Lundstrom, and A. W. Ghosh, "Generalized effective-mass approach for n-type metal–oxide–semiconductor field-effect transistors on arbitrarily oriented wafers," *J. Appl. Phys.*, vol. 97, no. 5, pp. 053 702–053 713, Feb. 2005.

[19] F. Stern and W. E. Howard, "Properties of semiconductor surface inversion layers in the electric quantum limit," *Phys. Rev.*, vol. 163, no. 3, pp. 816–835, Nov. 1967.

[20] A. Rahman, J. Guo, S. Datta, and M. S. Lundstrom, "Theory of ballistic nanotransistors," *IEEE Trans. Electron Devices*, vol. 50, no. 9, pp. 1853–1864, Sep. 2003.

Neophytos Neophytou (S'05) received the B.S. degree in electrical and computer engineering and the M.S. degree in the area of microelectronics and nanotechnology from Purdue University, West Lafayette, IN, in 2001 and 2003, respectively, where he is currently working toward the Ph.D. degree in the School of Electrical and Computer Engineering.

He is currently working on the effects of band structure on the electronic properties of nanowires as well as the effect of atomistic variations and defects in the transport on nanoscale devices. His research interests include computational modeling of quantum–mechanical electron transport through carbon nanotubes, nanowires, graphene-based channels, and new channel materials.

Gerhard Klimeck (S'94–M'96–SM'04) received the German Electrical Engineering degree from Ruhr-University Bochum, Bochum, Germany, in 1990, and the Ph.D. degree from Purdue University, West Lafayette, IN, in 1994.

He was the Technical Group Supervisor for the Applied Cluster Computing Technologies Group and continues to hold his appointment as a Principal Member with the NASA Jet Propulsion Laboratory on a faculty part-time basis. Previously, he was a Member of the Technical Staff with the Central Research Laboratory, Texas Instruments. He is currently the Associate Director for Technology of the Network for Computational Nanotechnology and a Professor with the School of Electrical and Computer Engineering, Purdue University. He leads the development and deployment of web-based simulation tools that are hosted on http://nanohub.org—a community website that is utilized by over 26 000 users annually. He has been the lead on the development of NEMO 3-D, which is a tool that enables the simulation of tens-of-million atom quantum dot systems, and NEMO 1-D, which is the first nanoelectronic computer-aided-design tool. His work is documented in over 180 peer-reviewed publications and over 310 conference presentations. His research interests include modeling of nanoelectronic devices, parallel cluster computing, and genetic algorithms.

Dr. Klimeck is a member of American Physical Society, Eta Kappa Nu, and Tau Beta Pi. More information can be found at http://www.ece.purdue.edu/~gekco and http://nanoHUB.org/klimeck.

Mark S. Lundstrom (S'72–M'74–SM'80–F'94) received the B.S. and M.S. degrees in electrical engineering from the University of Minnesota, Minneapolis, in 1973 and 1974, respectively, and the Ph.D. degree in electrical engineering from Purdue University, West Lafayette, IN, in 1980.

From 1974 to 1977, he was with the Hewlett–Packard Corporation, Loveland, CO, working on integrated-circuit process development and manufacturing support. Since 1980, he has been with the School of Electrical Engineering, Purdue University, where he is currently the Don and Carol Scifres Distinguished Professor with the School of Electrical and Computer Engineering and the Founding Director of the Network for Computational Nanotechnology. He was the Director of Purdue University's Optoelectronics Research Center from 1989 to 1993 and was the Assistant Dean of Engineering from 1991 to 1994. His current research interests center on the physics of small electronic devices, particularly nanoscale transistors, and on carrier transport in semiconductor devices.

Dr. Lundstrom currently serves as an IEEE Electron Devices Society Distinguished Lecturer. He is a Fellow of the American Physical Society and the American Association for the Advancement of Science. In 1992, he received the Frederick Emmons Terman Award from the American Society for Engineering Education. He and his colleague, S. Datta, received the 2002 IEEE Cledo Brunetti Award for their work on nanoscale electronic devices. In the same year, they received the Semiconductor Research Corporation's Technical Excellence Award. In 2005, he received the Semiconductor Industry Association's University Researcher Award for his career contributions to the physics and simulation of semiconductor devices. Most recently, in 2006, he was the inaugural recipient of the IEEE Electron Devices Society's Education Award.

Yang Liu (S'05) received the B.S. degree in applied physics from the University of Science and Technology of China, Hefei, China, in 2003, and the M.S. degree in mechanical engineering from Purdue University, West Lafayette, IN, in 2005, where he is currently working toward the Ph.D. degree in the School of Electrical and Computer Engineering.

He is currently working on band-structure effects on the performance of nano-MOSFETs in Si as well as new channel materials and structures. His research interests are modeling quantum transport in nanoscale devices.